UCRL-92355
PREPRINT

CIRCULATION COPY
SUBJECT TO RECALL
IN TWO WEEKS

A MULTIPHASE CONTINUUM MODEL TO DESCRIBE DYNAMIC LOADING EFFECTS IN NONLINEAR POROUS MEDIA

R. P. Swift
D. E. Burton
J. B. Bryan
H. D. Glenn

This paper was prepared for presentation at the Symposium on Response of Geologic Materials to Blast Loading and Impact, 1985 Joint ASME/ASCE Summer Mechanics Conference, Albuquerque, NM, June 24-26, 1985.

March, 1985

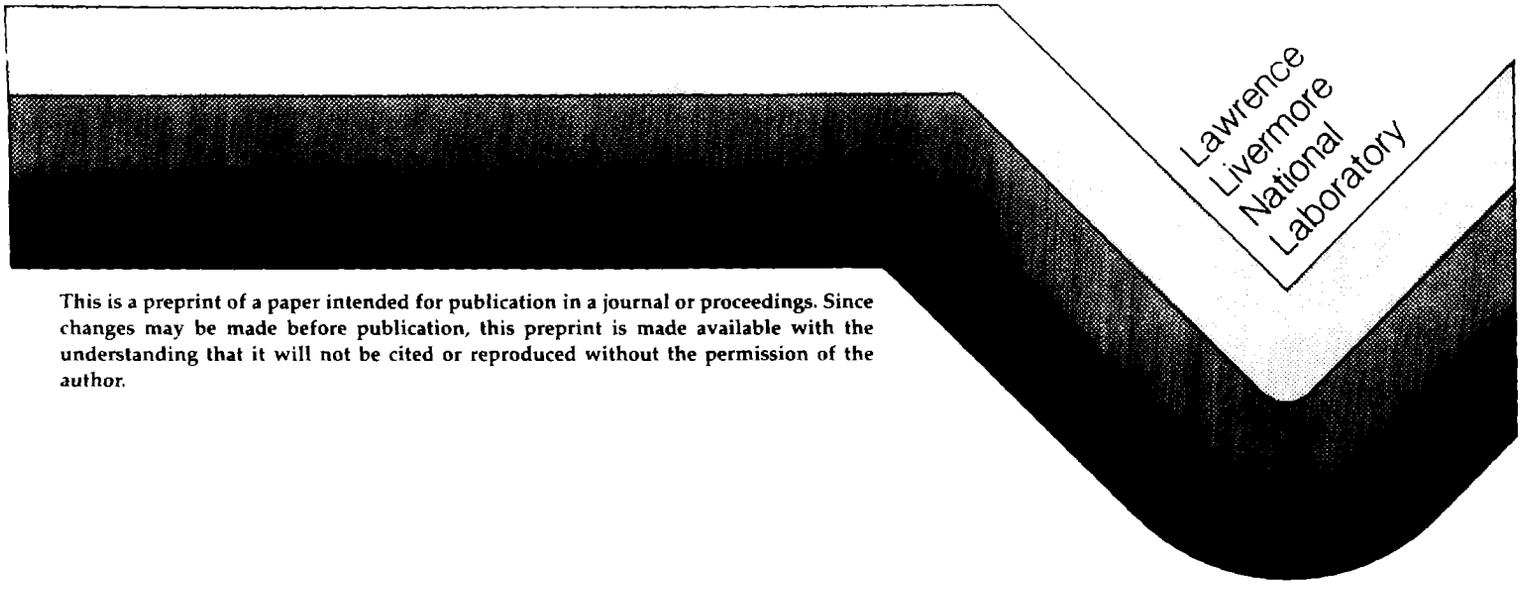

This is a preprint of a paper intended for publication in a journal or proceedings. Since changes may be made before publication, this preprint is made available with the understanding that it will not be cited or reproduced without the permission of the author.

DISCLAIMER

This document was prepared as an account of work sponsored by an agency of the United States Government. Neither the United States Government nor the University of California nor any of their employees, makes any warranty, express or implied, or assumes any legal liability or responsibility for the accuracy, completeness, or usefulness of any information, apparatus, product, or process disclosed, or represents that its use would not infringe privately owned rights. Reference herein to any specific commercial products, process, or service by trade name, trademark, manufacturer, or otherwise, does not necessarily constitute or imply its endorsement, recommendation, or favoring by the United States Government or the University of California. The views and opinions of authors expressed herein do not necessarily state or reflect those of the United States Government or the University of California, and shall not be used for advertising or product endorsement purposes.

A MULTIPHASE CONTINUUM MODEL TO DESCRIBE DYNAMIC LOADING EFFECTS IN NONLINEAR POROUS MEDIA

Robert P. Swift, Physicist
Donald E. Burton, Physicist
Jon B. Bryan, Physicist
H. David Glenn, Physicist
Earth Sciences Department
Lawrence Livermore National Laboratory
Livermore, California 94550

ABSTRACT

A multiphase constitutive model that couples nonlinear deformation to porous flow has been developed for numerical analyses of dynamic behavior of geological media. The model has been incorporated into the explicit finite-difference code TENSOR and applied to examine the phenomenology associated with contained explosions and nuclear surface cratering in a coral geology. For contained explosions in nearly saturated media, the model predicts a region of liquefaction to exist adjacent to the cavity. This region is markedly enhanced for the case of total saturation and the associated pore pressure buildup indicate that the stability of the residual stress field may be threatened. Based on plausible assumptions about the geology and the constitutive relations of coral, we have shown that the multiphase constitutive model can relate subsidence to calculational parameters such as peak effective stress. Most of the observed volume of the Koa crater at the Pacific Proving Grounds can be accounted for by late time consolidation of the damaged coral.

INTRODUCTION

Geological materials consist of an assemblage of particles of different sizes and shapes that form a matrix whose voids are filled with fluids. In general, such materials must be viewed as two-phase (saturated) or multiphase materials whose state is dependent on the stresses and deformation within each phase. The stresses carried by the porous matrix are conventionally termed "effective stresses" and those in the fluid phase are called "pore pressures". When free drainage conditions exist, the steady state pore pressure of the fluid depends only on the hydraulic conditions and is independent of the response of the matrix to external loads. However, in most cases in which some flow can occur or even when undrained conditions prevail, there is an interaction between constituents, such as the coupling of matrix deformation to pore-fluid flow and pore pressure. Proper examination of such cases requires explicit treatment of the interactions of each phase, such as in the compaction of saturated media, consolidation, liquefaction, and the transient flow of pore fluids through voids and fissures. The solutions to such problems require a multiphase continuum description of the porous media. Two areas that warrant attention to multiphase behavior are the containment of underground explosions and crater formation resulting from high-yield nuclear surface bursts. This paper illustrates the application of a multiphase continuum model to examine these phenomena.

Over the past two decades, a great amount of effort has been expended to understand the containment phenomenology associated with underground explosions (1-4). A specific need still exists to improve our understanding of the influence of water pore pressure during shock passage and slightly later during the development of the residual stress field (i.e., "containment cage") that forms around an explosion-produced cavity. Other needs are to determine the degree of containment cage deterioration as a result of the subsequent pore fluid migration process, to define the potential for cavity gas migration through the degraded containment cage region, and to identify the dependence of cavity collapse and subsidence on pore-pressure effects. These containment-related processes are highly nonlinear and depend on the interactions of individual constituent phases.

To understand the effectiveness of nuclear weapons, one must be able to predict the effects of near-surface detonations of relatively high-yield nuclear devices (several hundred kilotons) on targets embedded in various kinds of rocks and soils. However, all of the high-yield explosive cratering events in the U.S. data base took place at the Pacific Proving Grounds (PPG). The PPG are located at the Enewetak and Bikini atolls. The geology of these coral atolls is unlike that of any continent. The matter is not academic; empirical formulas used until recently to predict the size and shape of weapon craters (5) are based on data from the PPG. We now believe that these formulas greatly over-estimate surface-burst effectiveness in typical continental geologies.

There have been so few above-ground and shallow-buried nuclear events that it has been necessary to develop numerical techniques to extrapolate beyond known craters to predict the effects of new weapons and new geologic settings. Some doubt remains about the completeness of such models because of their inability to reproduce the very shallow, saucer-shaped craters formed in coral at the PPG. Calculated crater volumes in studies by some investigators are only about 20 to 25% of those observed in coral, and none have reproduced the shapes associated with these events. For example, Figure 1 contrasts the result of a typical numerical simulation (6) with the profile of the Koa event crater (7) which has a volume of 2.11×10^7 m^3 and radius of about 600 m. Of the several physical mechanisms that have been postulated for the size and shape of the Pacific craters (8), the most plausible involves the geological peculiarities of the PPG which are not usually encountered in the continental U.S. geology and which may involve physics not included in previous models. Unlike continental soils, coral is saturated, highly porous, and permeable. This suggested to us that an explanation of crater shapes in coral involves the effects of pore pressure and porous flow.

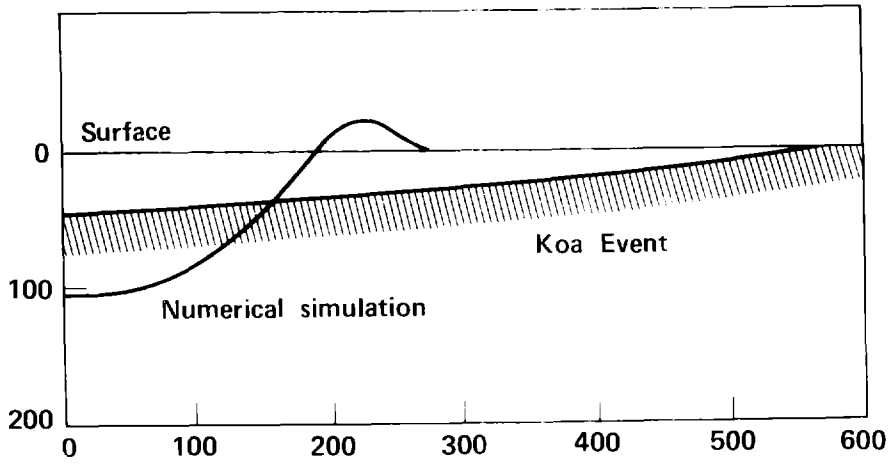

Fig. 1. Profile of a Pacific Proving Ground Crater (Koa Event) contrasted with the crater resulting from a typical numerical simulation (6).

In this work, we have developed a multiphase constitutive model based on mixture theory (9), and incorporated it into our two-dimensional continuum dynamics code TENSOR (10). To illustrate the broad range of application we present the simulation of some small-scale, contained high explosive experiments conducted in grout spheres (11) and then present a simulation of the 1.3 Megaton (Mt) Koa nuclear event conducted at the PPG. For contained explosions, our studies (12) indicate that the formation of a residual stress field around the explosive created cavity is markedly degraded in a fully saturated region. The shock-induced pore pressure causes tensile failure to occur outward from the cavity, creating a region of liquefaction (loss of shear strength) and precluding development of a residual stress field in the liquefied region. The extent of the liquefied region is greatly reduced by a small amount of initial air filled porosity. In our cratering study (13), the size and shape of the Koa crater are attributed to late-time subsidence and liquefaction effects. Following passage of the shock wave the pore fluids migrate upwards through the fractured coral, and the coral consolidates to a volume comparable to that attained during shock passage. The accumulated consolidation leads to surface subsidence which enlarges the early bowl-shaped transient crater. Shock liquefaction was also predicted in the calculations with our model; liquefied coral can be expected to slump and slowly transform bowl-shaped craters into the saucer shaped craters that were observed.

MULTIPHASE CONSTITUTIVE RELATIONSHIPS

The constitutive model assumes a solid containing two types of flaws: pores considered to be preexisting, isotropic, and homogeneous, and cracks that are induced during the calculation and treated using an anisotropic algorithm (14). Although we make a logical distinction between crack and pore pressure, the assumption of pressure equilibrium between the two types of flaws reduces the system to three components (solid, water, and air). A complete discussion of the multiphase model is given in (9). The following briefly describes the types of relationships which govern the system response.

Kinematic Conditions

The kinematic conditions needed for a solid (s), water (w), air (a), multiphase material are

$$M_s = \rho_s (1 - \phi) V, \quad M_w = \rho_w S \phi V, \quad \text{and} \quad M_a = \rho_a (1-S) \phi V \tag{1}$$

in which M_i is mass, ρ_i is density, V is volume, and the saturation, porosity, and the constituent porosities are defined by

$$S = \phi_w/\phi, \qquad \phi = \phi_w + \phi_a, \qquad \text{and} \qquad \phi_i = V_i/V. \tag{2}$$

Constituent Response Laws

The constituent response laws are normally given as tabular functions in terms of stress, σ_i, versus density, ρ_i, while the low pressure water and air responses are represented by adiabatic gas law approximations,

$$\sigma_w = \sigma_w (\rho_w), \qquad \sigma_a = \sigma_a(\rho_a), \qquad \text{and} \qquad \sigma_s = \sigma_s(\rho_s) \tag{3}$$

Constraints

Pressure equilibrium is assumed between the water and air and between the pores and cracks. These constraints can be recast as functions of S and ϕ or

$$\sigma_w (\phi, S) = \sigma_a(\phi, S). \tag{4}$$

Effective Stress Law

The final volumetric relationship is provided by the effective stress law. The classical concept of effective stress was due to Terzaghi (15) and suggests that the bulk response of a porous solid can be separated into that due to the pore fluid and that due to an "effective" stress defined as

$$\sigma_e = \sigma - \sigma_f \tag{5}$$

with

$$\sigma_f(\phi,S) = S\,\sigma_w + (1-S)\,\sigma_a, \tag{6}$$

where σ is the total stress tensor. The Terzaghi effective stress has been shown (9) to satisfy a response law of the form

$$\dot{\sigma}_e = K\left(\dot{\epsilon} - \frac{\dot{\sigma}_f}{K_s}\right), \tag{7}$$

where K and K_s are the drained and solid bulk moduli and $\dot{\epsilon} = \dot{V}/V$ is the volumetric strain rate and the term in parentheses appears as an effective strain rate.

Although the effective stress response law for σ_e is convenient for purposes of understanding, it has several embedded singularities that must be removed in the numerical implementation. It can be shown that the response law reduces to the following form, (9)

$$(1-\phi)\left(1-\phi-\frac{K}{K_s}\right)\left[\dot{\epsilon} - \frac{\dot{\sigma}_f(S,\phi)}{K_s}\right] - \left[1-\phi+\frac{\sigma_e(S,\phi)}{K_s}\right]\dot{\phi} = 0. \tag{8}$$

The pore collapse model presently employed in the TENSOR code is functionally similar to a P-α model (16), with the major addition of tensile failure algorithms that produce volume dilatancy. In the above form the theory is reduced to solving two equations (4) and (8) simultaneously for saturation, S, and total porosity, ϕ, at each time step. This is done using a modified Newton-Raphson iteration scheme. This provides a trial value for σ_e, which then becomes input for the failure algorithms that depend on deviatoric response as well as on volumetric response.

Deviatoric Response Laws

The above discussion focused on the volumetric properties of the multiphase system. It is well known that an increase in fluid pressure can lower the failure strength of a saturated or partially saturated soil or rock and that the strength can be described in terms of effective stress, (17,18). Following this tradition our multiphase failure model was formulated in terms of the drained strength of the porous material and the effective mean stress, σ_e, which is simply substituted for the total mean stress, σ, to account for pore pressure effects. The failure surface is assumed to have the form

$$F(\bar{\sigma}_e,\ J_2^{1/2}) = 0 \tag{9}$$

with

$$\bar{\sigma}_e = \sigma_e - \left(\frac{J_3}{16}\right)^{1/3}, \tag{10}$$

where $J_2 = (S_{ij}S_{ij}/2)$ and $J_3 = (S_{ij}S_{ik}S_{kj}/3)$ are the second and third deviatoric stress invariants, respectively, and S_{ij} are components of the deviatoric stress tensor. The quantity $\bar{\sigma}_e$ accounts for the intermediate principal stress and allows a single yield surface (9) to approximate the failure behavior of geological materials that are generally different in compression and extension (19).

The process of failure and/or yielding is accommodated by a flow rule that has been included in TENSOR (10). The flow rule specifies the form of inelastic strain rates, $\dot{\epsilon}^I$, or inelastic stress rates, $\dot{\sigma}^I$, and can depend on one or more control surfaces. These control surfaces are typically a failure surface $F(\sigma_{ij}) = 0$, as in (9), and a loading potential surface $G(\sigma_{ij})$, which is often taken equal to F.

As in many elastic-inelastic models the total strain rate, $\dot{\epsilon}_{ij}$, is separated into its elastic and inelastic parts,

$$\dot{\epsilon} = \dot{\epsilon}^E + \Sigma\,\dot{\epsilon}^I, \tag{11}$$

whose sum is over the number of inelastic processes, such as shear yielding, tensile failure, etc. A trial value of effective stress, σ_e^T, is obtained from (8) by assuming that the effective stress rate reflects only the elastic contribution and the correction for solid compressibility (i.e., $\dot{\epsilon} = \dot{\epsilon}_e^E$). The true effective stress resulting from (7) and (11) is

$$\dot{\sigma}_e = K(\dot{\epsilon} - \dot{\sigma}_f/K_s) - \Sigma K \dot{\epsilon}^I = \dot{\sigma}_e^T - \Sigma\dot{\sigma}_e^I , \qquad (12)$$

where σ_e^I are the inelastic effective stresses, which are corrections determined by the failure algorithm. As noted previously, the trial values for σ_e^T are obtained by a Newton-Raphson iteration that solves for S and ϕ. The failure model imposes constraints on σ_e resulting in a value that is different from that obtained using the trial values for S and ϕ. It is in this manner, for example, that the void space produced by tensile failure enters into the total porosity ϕ. Numerically, this is accomplished by a second Newton-Raphson iteration for S and ϕ, but with the effective stress law (8) removed from the system of equations.

SHOCK INDUCED CONSOLIDATION AND LIQUEFACTION

The presence of water in porous rock or soil greatly affects both the transient and late-time material response and leads to the effects of consolidation and liquefaction. When the material is dry it transmits shock poorly; the crushing and collapse of its pores attenuates the shock rapidly with distance, concentrating damage to the region near the source. Pores filled with water transmit shock better than air-filled pores, so the shock travels with less attenuation and can damage larger volumes of material far from the source.

Figure 2 illustrates typical responses of drained and undrained shocked porous material. In Figure 2a, which illustrates the consolidation processes, the drained material matrix starts with an initial effective stress shown at point A. As the shock wave traverses the material, it first compresses this drained matrix to point B (irreversibly compacting it) and then unloads down the release path through to the axis (where the material fails in tension) and then to point C.

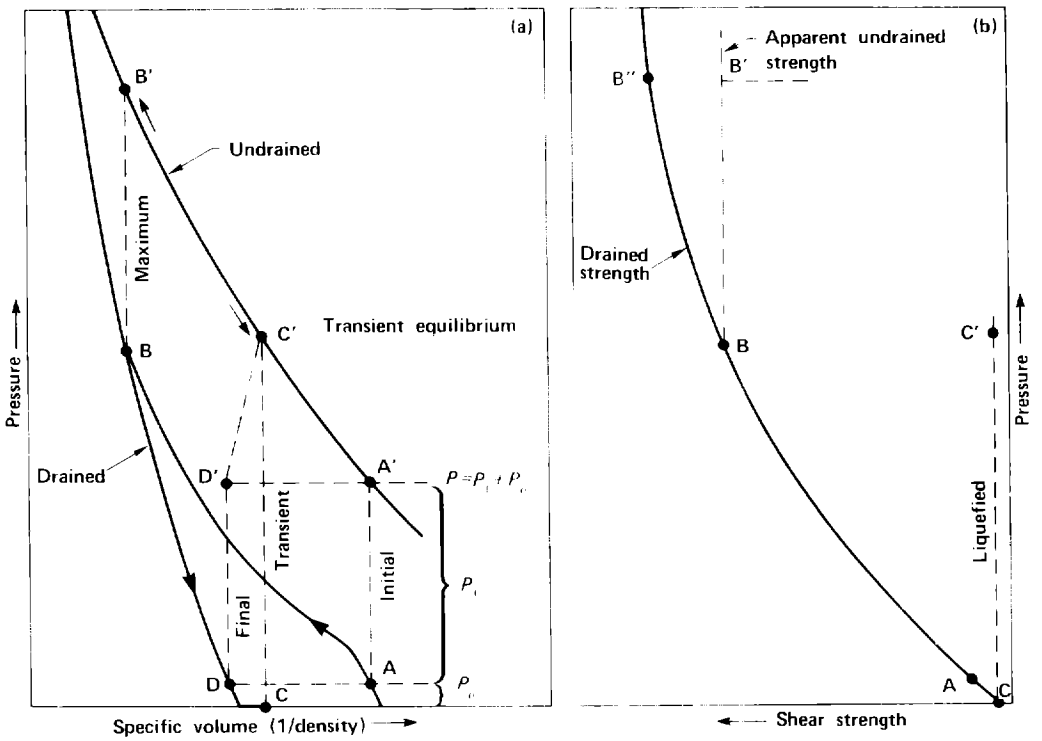

Fig. 2. Curves illustrating the compaction and liquefaction processes. (a) Specific volume versus pressure. (b) Shear strength versus pressure.

Mixture theory enables us to describe the response of undrained porous media in terms of the drained material response at corresponding volumetric strains. (For simplicity in this discussion, we ignore the small volumetric correction due to the compressibility of the solid grains.) For undrained material, the shock response would be to move from point A' to the shocked condition (point B') corresponding to the strain in a drained state (point B). The corresponding degree of unloading for the undrained material is point C', at which time the material motion has slowed and is in a transient equilibrium state with respect to total stress.

Final equilibrium with respect to effective stress occurs by porous flow. Although we are not at present modeling porous flow, we can infer the net effects using our model by assuming that the effective stress reloads back to its initial value (that is, the final and initial effective pressures are approximately the same). Because the release path BD is steep compared to BA, volume errors resulting from the effective pressure approximation are relatively small. The maximum effective pressure for each zone is monitored and used to obtain the release path BD and the final equilibrium volume. For instance, if a calculation is stopped at point C' (corresponding to the specific volume at point C for dry material), the net consolidation or volume change for each zone can be determined by going from point C back to point D. The final state for the system is point D'.

The consolidation volume is simply the difference between the transient (C) and final (D) volumes. For surface explosions the surface subsidence at a given distance from the center of the detonation is determined by adding the calculated consolidation changes for all the zones at that radius vertically. Plotting these results as a function of radius from the detonation will provide a subsidence profile for the crater. We can then calculate the total volume of the subsidence crater by integrating over the subsidence profile.

Mixture theory also indicates that the apparent shear strength is changing continuously during the shock loading and unloading process. This is illustrated in Figure 2b, which gives the pressure-shear stress behavior for conditions corresponding to the pressure-specific volume behavior in Figure 2a. When the material is shocked to a high pressure (point B'), the effective pressure has increased to point B. A saturated material thus appears weaker (B') than a dry material at the same total pressure (B'') because the porous material fails at B. At the peak of the shock, the shear strength of the saturated material is limited by the curve ABB'.

At a later stage in the loading, after the shock wave passes, the shear strength will be limited by the curve CC' near zero, resulting in a condition known as liquefaction. In terms of the mixture model, the liquified strength CC' results because the effective pressure lies at point C on the drained-strength curve. Physically, this arises because, as the effective pressure unloads to point C, the porous material grains are forced apart by the fluid although the total stress is still compressive. Thus, material particles may find themselves suspended (surrounded by water) resulting in a lack of cohesion. The present mixture constitutive model is inadequate to treat such slurry-like behavior.

CALCULATIONS OF CONTAINED EXPLOSIONS

We used contained explosive experiments performed in a nearly saturated, low permeable rock simulant (11) as one test case for our multiphase model. The experiments were performed in 0.28 m diameter spheres surrounded by water pressurized to 6.9 MPa. A 0.0127 m diameter charge of PETN with a density of 1000 kg/m^3 was detonated at the center of the sphere and radial particle velocity measurements were obtained at various radii from the explosive source. Average physical properties of the grout were as follows: grain density = 2976 kg/m^3, dry density = 1815 kg/m^3, porosity = 39%, water by weight = 17.4% and air filled porosity varied from 0.0 to 1.1%. The parameter values used in the multiphase model were determined by fitting the model to static triaxial and uniaxial strain data obtained in (20). The numeric simulations of spherical wave propagation in grout were carried out with TENSOR. Details of the calculations are given in (9).

Good agreement of the calculated particle velocity response with experimental data was obtained by assuming an air-filled porosity of 0.8%, at radii of 0.019, Figure 3a, and 0.04m, Figure 3b. Figure 4 compares the response calculated for fully saturated conditions with experimental data at a radius 0.019 m. The higher calculated peak velocity, broadening of the positive phase of the wave, and modification to the negative phase are the result of reduced shock attenuation associated with fully saturated conditions and the increased buildup in pore pressure. The higher pore pressure leads to liquefaction of a larger region surrounding the cavity than for the partially saturated case.

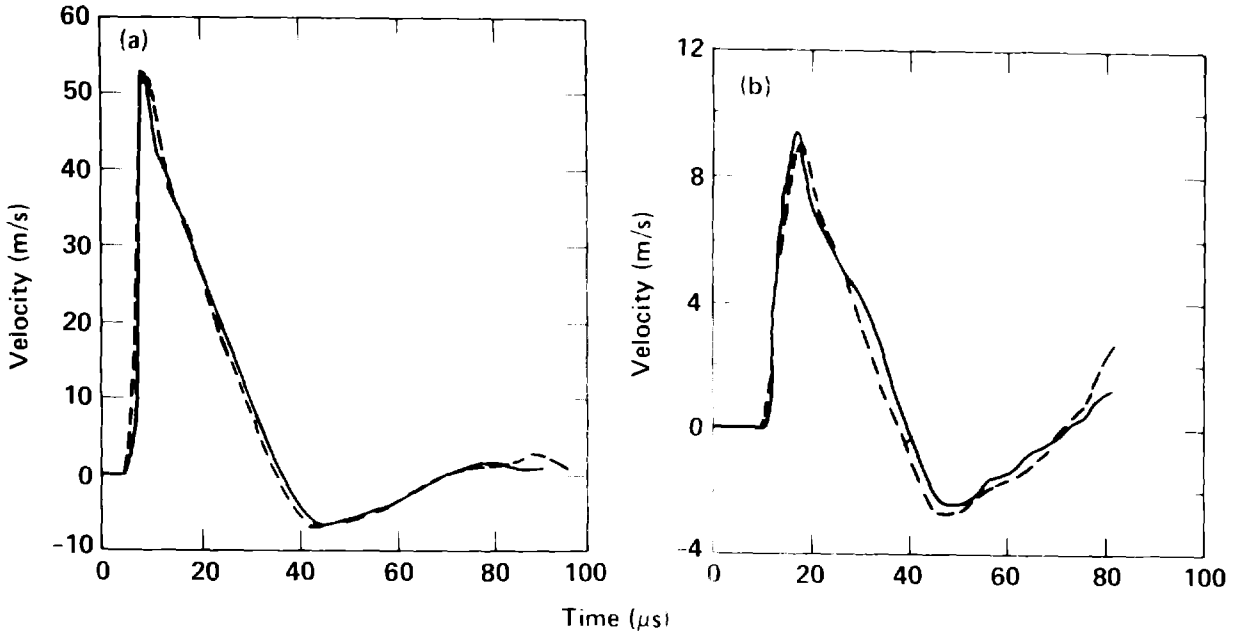

Fig. 3. Comparison of calculated (solid line) and measured (dashed line) particle velocity in grout sphere at radius of (a) 0.019 m and (b) 0.040 m for 0.8% air-filled porosity.

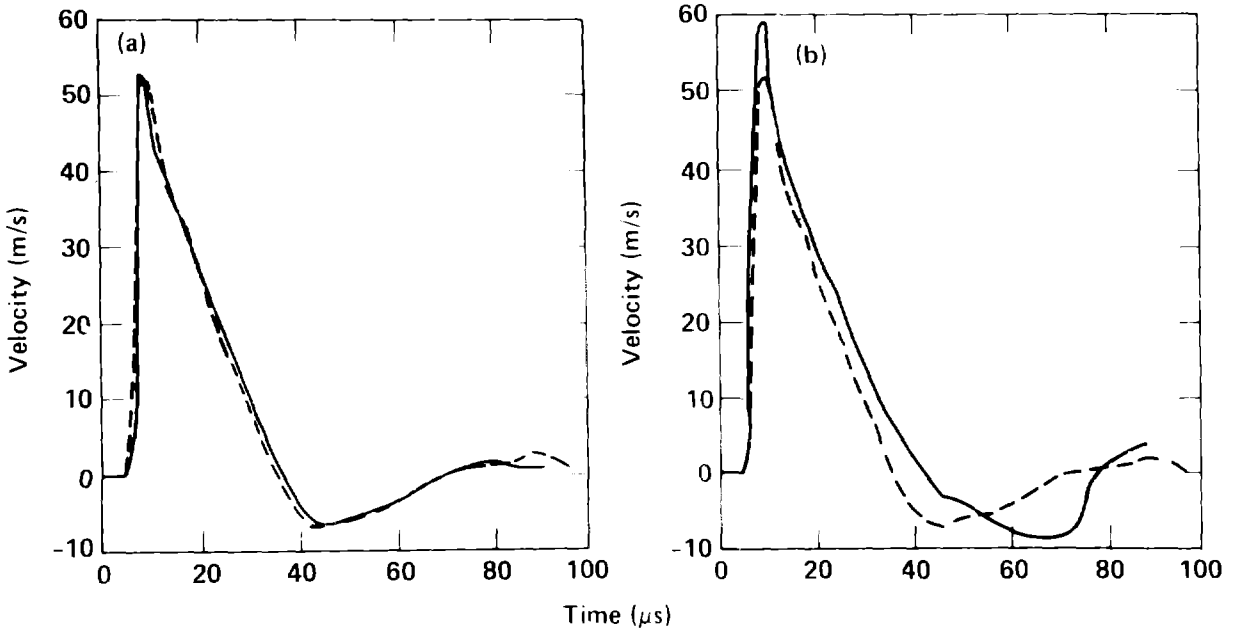

Fig. 4. Comparison of calculated (solid line) and measured (dashed line) particle velocity in grout sphere at radius of 0.019 m for (a) 0.8% air-filled porosity and (b) no air-filled porosity.

The stress response shown in Figure 5 at a radius 0.019 m clearly illustrated the effect of liquefaction. At about 42 μs behind the wave front, in Figure 5a, the radial and circumferential stress components equalize and remain so, indicating a loss of shear resistance. This contrasts with the classical stress wave forms shown in Figure 5b associated with spherical explosions using a single phase constitutive model, where stress reversal occurs leading to a residual stress field. The liquefaction is a result of pore-pressure-induced tensile failure which occurs during unloading because the stress in the matrix material unloads more rapidly than does the water pore pressure. Hence, the effective stresses become tensile causing the matrix to fail in tension (i.e., a tensile strength of 3.44 MPa was used for the grout).

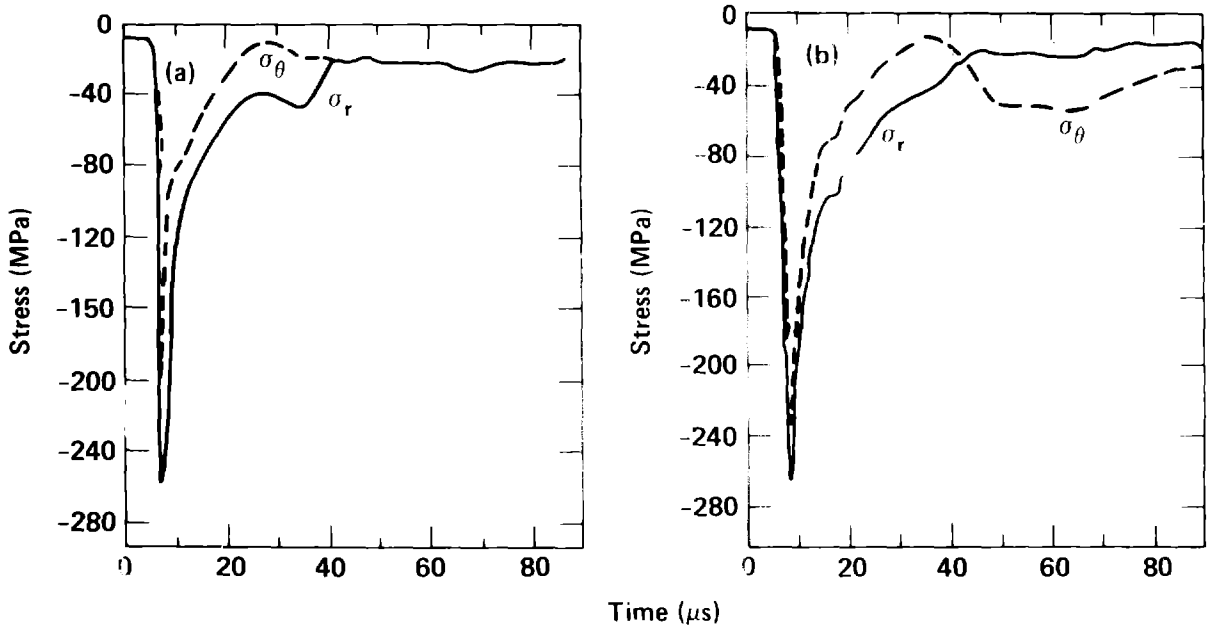

Fig. 5. Radial (solid line) and circumferential (dashed line) stress histories calculated at a radius of 0.019 m with (a) multiphase model and (b) that resulting from a single phase model.

A residual stress region, where stress reversal occurs, forms outside the liquefied region and is quite sensitive to the amount of air-filled porosity. This is illustrated in Figure 6 which shows radial stress, circumferential stress and pore pressure distribution at 90 μs. The residual stress field for the partially saturated case in Figure 6a somewhat resembles the field that could result from an explosion in a larger initial cavity whose final radius is comparable to the extent of liquefaction. Under total saturation, in Figure 6b, the region of liquefaction is increased, the residual stress region is displaced farther out from the cavity, and the magnitude of residual stresses are considerably lower than the pore pressure in the liquefied region.

The high pore pressure in the liquefied region around the cavity may be a liability to the stability of the residual stress field for the fully saturated case. To assess this threat requires modeling of late-time fluid migration and of the relaxation of excess pore pressure and its effect on the residual stress field. This was addressed here by hypothetically relaxing the pore pressure in each zone from its value at 90 μs to its initial lithostatic value at a rate of 0.4% per cycle. The lithostatic pore pressure for the air-filled porosity case was 0.1 MPa, and that for the saturated case was 1.65 MPa. We assumed that cavity pressure was also relaxed to the lithostatic stress. The adjusted residual stress distributions for the 0.8% air-filled porosity and fully saturated conditions are shown in Figures 7a and 7b, respectively. The results indicate that a small amount of air-filled porosity greatly improves the formation of the residual stress cage and that explosions in fully saturated regions may be more susceptible to unstable behavior.

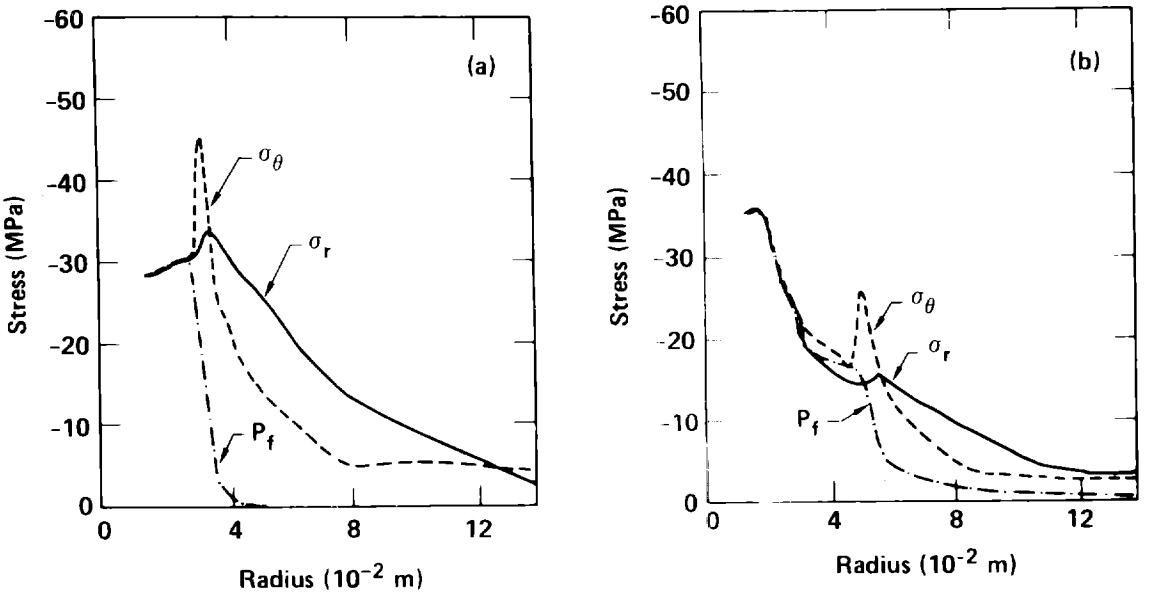

Fig. 6. Radial (solid line) and circumferential (dashed line) stress and pore-pressure (dash-dot line) distributions at 90 μs calculated with (a) 0.8% air-filled porosity and (b) no air porosity.

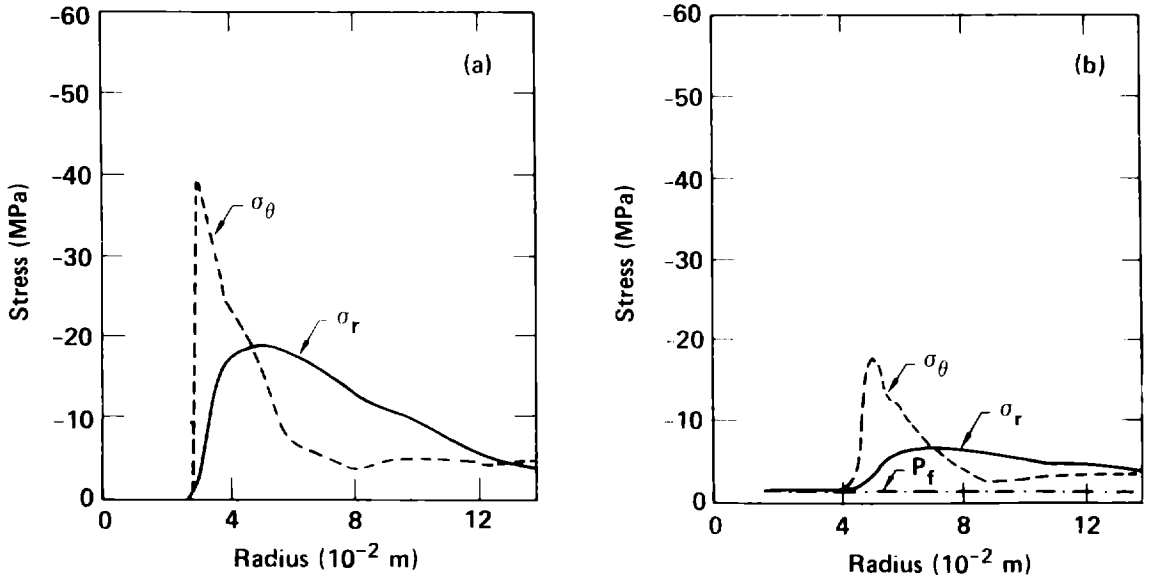

Fig. 7. Residual stress distribution for radial (solid line) and circumferential (dashed line) stress after relaxation of pore pressure to 0.1 MPa for (a) 0.8% air-filled porosity and (b) no air-filled porosity.

SIMULATING THE KOA EVENT

We used the large crater produced by the Koa event (2.11 x 10^7 m^3 in apparent crater volume) as another test case for our multiphase model. The 1.3 Mt Koa device was detonated in a tank of water placed on a concrete pad poured over coral sand. We modeled the various layers of coral below the ground surface to a depth of 1300 m using measured densities and compressional velocities. Five types of coral were identified and the geologic profiles were obtained for the bulk density and compressional velocity as a function of depth. These profiles were constructed from density logs, core samples, and seismic velocity records.

The calculation was begun with an Eulerian code, which treates the radiation-hydrodynamic energy transfer at early times. The Eulerian code was run to a time of 1 ms and then linked to the Lagrangian code TENSOR. We mapped the pressures, densities, and velocities calculated by the Eulerian code onto a larger grid that extended to a depth of 50 m and a radius of 200 m and continued the calculations with the TENSOR code. After the link, the airblast loading on the ground surface was approximated by a pressure boundary condition due to (21). We repeated this overlay procedure six times. The final TENSOR grid extended to a depth of 1300 m and a radius of 1400 m.

Figure 8 illustrates the overlaying process, the scale of the problem, and the propagation dynamics of the ground shock. The small black square around the origin at the upper left rear represents the region depicted at early times < 1 ms. The six TENSOR grids appear arrayed along the time axis according to the times of the ground-shock pressure contours shown (2, 10, 57, 133, 180, and 500 ms). The boundaries of the final TENSOR grid extend beyond the border of the figure. At about 45 deg from the surface, the effect of downward-traveling rarefaction waves generated by the free surface is evident in the shape of the pressure contours. The confinement of the peak pressures to a conical region about the symmetry axis is important to the subsidence interpretation that follows.

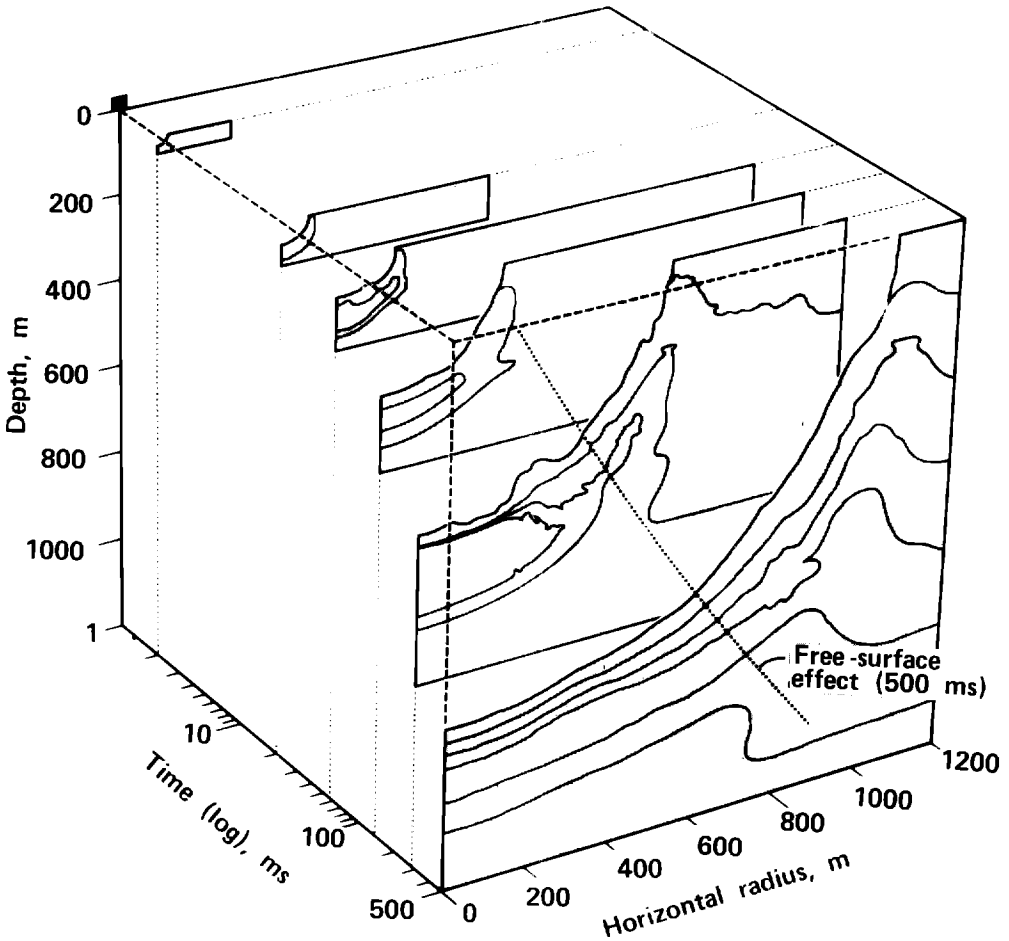

Fig. 8. The complete calculation of the Koa Event, starting with the Eulerian calculation (small square at the origin of the back plane) and continuing through six successive remappings to larger grids and TENSOR calculations. Pressure contours are shown for times of 2, 20, 57, 133, 280, and 500 ms.

Figure 9 shows contours of volumetric consolidation in relation to the various coral layers in the TENSOR mesh. These contours were obtained as discussed previously, by assuming the equality of initial and final effective stress (points A and D in Fig. 2). Note that the shape of the contours corresponds to the shock-propagation contours of Fig. 8 that exhibited the strong influence of rarefaction effects off the free surface. Most of the consolidation occurred within the observed crater radius, but significant contributions occurred for the relatively porous layer at a depth between 610 and 760 m.

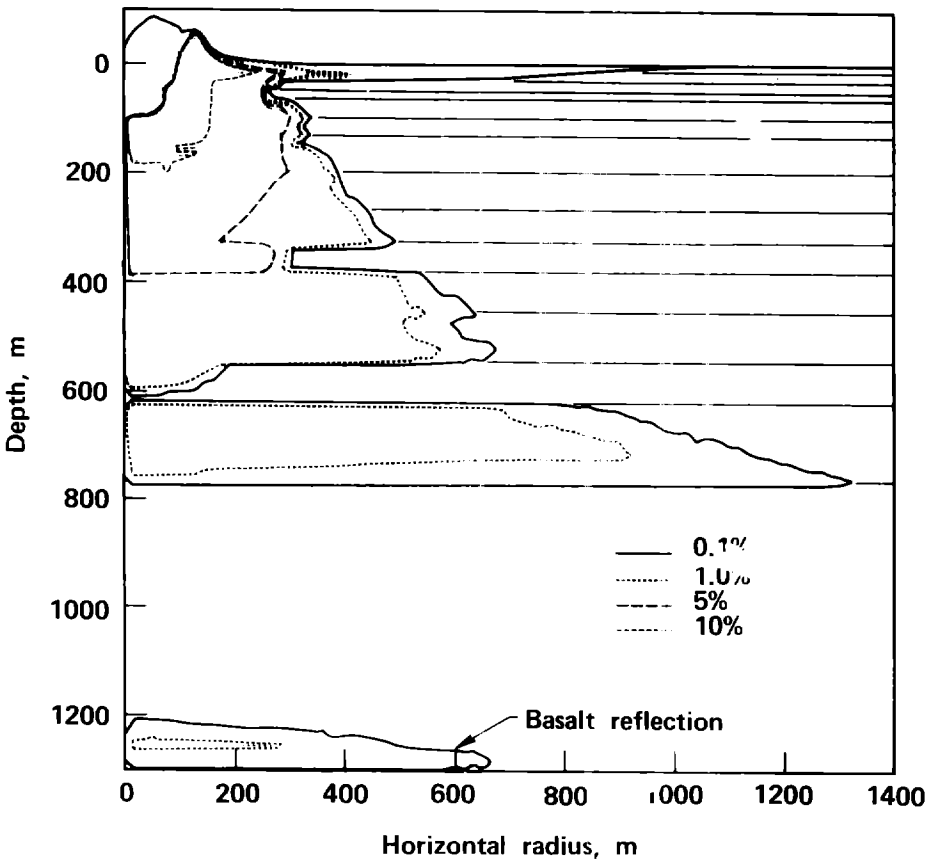

Fig. 9. Consolidation contours within the various coral layers. Numbers indicate volume change in percent. The consolidation in any given zone is a function of the local porosity and the peak shock stress.

Figure 10 presents the Koa event crater profile, measured along the reef, and at various phases of our calculation. The dashed curve represents the transient crater profile in the calculation at a time of 676 ms. The transient crater radius at this time was about 100 m.

Although the ground motion continued until at least 3.3 s (6), we terminated the calculation at 676 ms because we had carried it far enough to address the subsidence issue, which is governed primarily by the magnitude of the peak stress. We plan additional calculations out to later times, but for this study we have simply made a ballistic extrapolation to arrive at the modified solid profile shown in Fig. 10 to account for the influence of ejecta.

Combining our subsidence contribution with the ejecta profile, we obtain a third profile with a crater volume of 2×10^7 m^3, which is in excellent agreement with that of the actual crater, even though it has a different shape. Significant vertical displacements occur out to a radius of 500 m before rapidly tapering off.

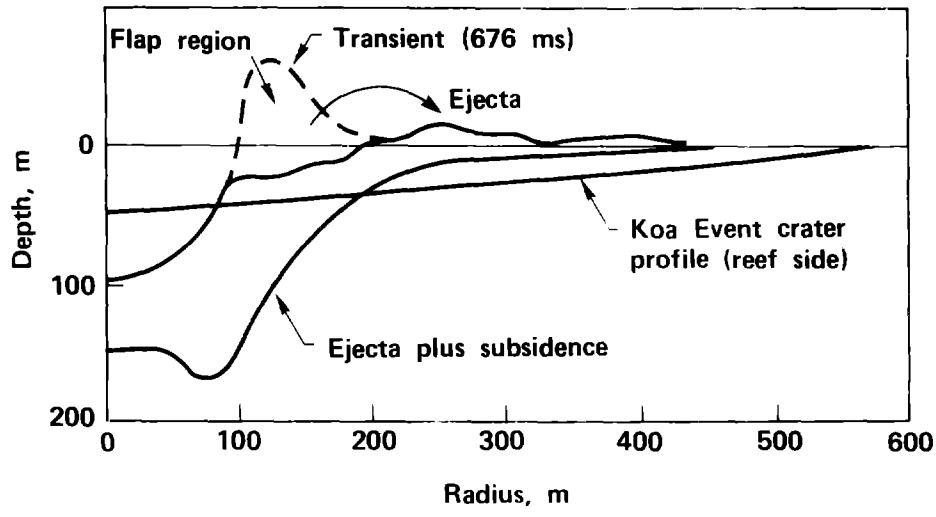

Fig. 10. Actual and calculated profiles for the Koa Event crater. Long and short dashes respectively represent the calculated transient profile and the EJECT calculation of throw-out. The solid curve is the crater profile resulting from vertical subsidence, which closely matches the volume of the observed Koa Event crater.

The indicated crater shape is an artifact of assuming that the subsidence is only vertical. The constitutive model predicts that the shear strength of the liquefied material will be insufficient to support a crater of this depth, so that at some time there would be a horizontal flow that fills in the crater. We have made no attempt to model this slumping in this study, since it is the transient crater, not its final form, that is important in strategic effects. However, it does seem clear that liquefaction would transform the bowl-shaped crater into a shallow saucer like the one observed.

REFERENCES

1. Rapp, E.G., "Containment of Buried Nuclear Explosions," UCRL-50604, 1968, Lawrence Livermore National Laboratory, Livermore, CA.

2. Terhune, R.W., "Analysis of Burial Depth Criteria for Containment," UCRL-52395, 1978, Lawrence Livermore National Laboratory, Livermore, CA.

3. Hudson, B.C., Jones, E.M., Keller, C.E., and Smith, C.W., Eds., Proceedings of the Monterey Containment Symposium, Los Alamos National Laboratory, Los Alamos, NM, 1981.

4. Olsen, C.W., Ed. Proceedings of 2nd Symposium for Containment of Underground Nuclear Explosions, Lawrence Livermore National Laboratory, Livermore, CA 1983.

5. Cooper, H.F., Jr., "A Summary of Explosion Cratering Phenomena Relevant to Meteor Impact Events," Impact and Explosion Cratering, Eds., D.J. Roddy, R.D. Pepin, and R.B. Merrill, Pergamon Press, New York, 1977.

6. Schuster, S.H., and Koit, V.E., "Initial KOA Calculations," Seventh Meeting of the DNA Ad Hoc Cratering Working Group, R&D Associates, Marina del Rey, CA, November 1983.

7. Ristvet, B.L., "Geologic and Geophysical Investigations of the Eniwetok Nuclear Craters," AFWL-TR-77-242, 1978, U.S. Air Force Weapons Laboratory, Kirtland Air Force Base, Albuquerque, NM.

8. Knowles, C.P. and Brode, H.L., "The Theory of Cratering Phenomena, an Overview," in Impact and Explosion Cratering, Eds. D.J. Roddy, R.D. Pepin, and R.B. Merrill, Pergamon Press, New York, 1977.

9. Swift, R.P., and Burton, D.E., "Numerical Modeling of the Mechanics of Non-linear Porous Media under Dynamic Loading," Lawrence Livermore National Laboratory, Livermore, CA, UCRL-53568, July 1984.

10. Burton, D.E., Lettis, L.A. Jr., Bryan, J.B., and Frary, N.R., "Physics and Numerics of the TENSOR Code," UCID-19428, 1982, Lawrence Livermore National Laboratory, Livermore, CA.

11. Cizek, J.C., and Florence, A.L., "Laboratory Investigation of Containment of Underground Explosions," SRI PYU-3876, 1982, SRI International, Menlo Park, CA.

12. Swift, R.P., and Burton, D.E., "Pore Pressure Effects in Contained Spherical Explosions," UCRL-91805, November 1984, Lawrence Livermore National Laboratory, Livermore, CA.

13. Burton, D.E., Swift, R.P., Bryan, J.B., and Glenn, H.D., "Subsidence in the Craters of Nuclear Tests at the Pacific Proving Grounds," Proceedings of the Engineering Foundation Conference on Compressibility Phenomena in Subsidence, Engineering Foundation Conferences, 1984.

14. Burton, D.E., Lettis, L.A. Jr., Bryan, J.B., Butkovich, T.R., and Bruce, A.L., "Anisotropic Creation and Closure of Tension Induced Fractures," UCRL-79578, 1977, Lawrence Livermore National Laboratory, Livermore, CA.

15. Terzaghi, K., Theoretical Soil Mechanics, Wiley, New York, 1943.

16. Hermann, W., "Constitutive Equations for Compaction of Porous Materials," Applied Mechanics Aspects of Nuclear Effects in Materials, Ed. C. C. Wan, ASME, New York (1971).

17. Brace, W.F., and Martin, R.J. III, "A Test of Effective Stress Law for Crystalline Rocks of Low Porosity," Intl. J. Rock Mech. Min. Sci., Vol. 5, 1968, p. 415.

18. Nur, A., and Byerlee, J.D., "An Exact Effective Stress Law for Elastic Deformation of Rock with Fluids," J. Geophys. Res., Vol. 76, 1971, p 6414.

19. Cherry, J.T., and Petersen, F.L., "Numerical Simulations of Stress Wave Propagation from Underground Nuclear Explosions," UCRL-72216, 1970, Lawrence Livermore National Laboratory, Livermore, CA.

20. Cooley, C.N., Smith, R.H., and Schatz, J.F., "Properties of Tuffs, Grouts and Other Materials," DNA 5986F, 1982, Defense Nuclear Agency, Washington, DC.

21. Brode, H.L., "Height of Burst Effects at High Overpressures," DASA 2506, 1970, update 1979, Defense Atomic Support Agency, Washington, DC.

This work was performed under the auspices of the U.S. Department of Energy by Lawrence Livermore National Laboratory under contract No. W-7405-Eng-48.